Numerical Prediction of Temperature Elevation Induced Around Metallic Hip Prostheses by Traditional, Split and Uniplanar Gradient Coils

Numerical Prediction of Temperature Elevation Induced Around Metallic Hip Prostheses by Traditional, Split and Uniplanar Gradient Coils

Luca Zilberti,[1] Oriano Bottauscio,[1] Mario Chiampi,[2] Jeffrey Hand,[3] Hector Sanchez Lopez,[4] Rüdiger Brühl,[5] and Stuart Crozier[4]

[1]Istituto Nazionale di Ricerca Metrologica, Torino, Italy.
[2]Politecnico di Torino, Dipartimento Energia, Torno, Italy.
[3]Division of Imaging Sciences and Biomedical Engineering, King's College London, London, U.K.
[4]School of Information Technology and Electrical Engineering, University of Queensland, St Lucia, Australia.
[5]Physikalisch-Technische Bundesanstalt (PTB), Berlin, Germany.

Correspondance to: Luca Zilberti, Istituto Nazionale di Ricerca Metrologica, Strada delle Cacce 91, I- 10135, Torino, Italy. E-mail: l.zilberti@inrim.it

Word count: 3739

Abstract

Purpose: The paper presents a computational study for the estimation of the temperature elevation occurring in a human subject carrying metallic hip prostheses when exposed to the magnetic field produced by gradient coils.

Theory and Methods: The simulations are performed through validated numerical codes, which solve the electromagnetic and thermal equations applied to a high-resolution anatomical human model. Three different sets of gradient coils (traditional, split and uniplanar) are considered to evaluate the maximum steady-state temperature elevation in the human body. This result is then rescaled to take into account the waveform of the signal, the duty-cycle and the duration of the scan.

Results: A number of exposure situations obtained by changing the patient's position is analyzed, finding temperature elevations on the order of some degrees.

Conclusion: The results are of possible concern and provide evidence of the need for further specific investigations aimed at assuring the safety of potential patients carrying metallic hip implants.

Keywords: temperature elevation, hip prostheses, gradient coils

INTRODUCTION

The annual rate of total hip arthroplasty procedures performed worldwide is on the order of one million; more than 160 procedures per 100,000 people are performed in most industrialised countries with numbers increasing by approximately 30% from 2000 to 2011 (1). The number of patients with orthopaedic implants undergoing Magnetic Resonance Imaging (MRI) is also increasing, due to the number of implants used and the availability of sequences that reduce artifacts (2). However, scanner manufacturers remain cautious regarding imaging of patients with implants and consider metallic implants a contraindication, unless the implant is labelled as MR conditionally safe. Although several reports describing either human exposure to gradient coils (3,4) or heating of hip prostheses due to the MRI radiofrequency (RF) fields have been published (5-9), the literature describing heating of such prostheses by switched gradient coils (GC) is relatively sparse. For example, Graf et al. (10) investigated heating in metallic structures including a titanium artificial hip and a replica made from aluminium exposed to a True-FISP sequence (maximum gradient: 40 mT/m, ramp time: 250 μs, dB/dt = 32 T/s, repetition time: 6.4 ms). The temperature of the more highly conducting aluminium replica increased by 2.2 °C after 210 s exposure whilst no measureable warming of the titanium device was observed. Such heating depends upon the geometry and physical properties of the implant, the distance from the isocentre and the switched gradient field sequence.

In a preliminary report, Sanchez-Lopez et al. (11) described the numerical simulation of heating of bilateral hip prostheses made from CoCrMo and Ti6Al4V alloys within a voxel body model exposed to the fields from conventional *x*-, *y*- and *z*-gradient coils.

In contrast to conventional GC, novel systems that combine MRI and a linear accelerator (MRI-LINAC) use modified gradient coils (12). Zilberti et al. (13) reported early results of numerical simulations of bilateral CoCrMo hip prostheses in an adult male voxel model exposed to the gradient coils of a MRI-LINAC, considering both axial and radial orientations of the body.

This work analyzes the temperature elevation induced in biological tissues due to the heating of two metallic hip implants exposed to three kinds of realistic gradient coils: traditional, split (suitable for MRI-LINAC platforms) and uniplanar. For each configuration, several patient positions have been modeled to explore a wide set of exposure situations, and the temperature elevation under steady-state conditions is computed via numerical simulations. Finally, a "rule of thumb" is provided, to allow estimation of the actual temperature elevation considering a verisimilar switching sequence and scan duration.

METHODS

Human Models with hip prostheses

The "Duke" body model (14), representing a 34-year-old male (height: 1.77 m, weight: 72.4 kg) is used in this study. It is composed of 77 biological tissues, whose properties (electric conductivity σ, relative permittivity ε_r, thermal conductivity λ, specific heat capacity *c*, blood perfusion rate *h* and density δ) have been taken from the database developed by the IT'IS Foundation (15). The model has been modified to include the presence of two different metallic hip implants. Both implants are generic, being representative

of typical real implants in dimensions and material composition. In the first case (Fig.1a), a unilateral right implant, including the acetabular shell and a liner, is considered. Its height, from the lower tip to the top of the femoral head is equal to 23 cm. The other model (Fig.1b), deduced from real CT images, represents a bilateral implant without acetabular shell and liner, whose total height is 22 cm. Two non-magnetic materials are considered for the metallic parts of the implants: a CoCrMo alloy (σ = 1.16 MS/m, ε_r = 1 , λ = 14 W/(m °C), c = 450 J/(kg °C), h = 0, δ = 8445 kg/m^3) or a Ti-6Al-4V alloy (σ = 0.58 MS/m, ε_r = 1 , λ = 7.2 W/(m °C), c = 520 J/(kg °C), h = 0, δ = 4420 kg/m^3). When present, the liner is made of polyethylene (σ = 0, ε_r = 2.25, λ = 0.47 W/(m °C), c = 1900 J/(kg °C), h = 0, δ = 940 kg/m^3). In a first approximation, the electric and thermal properties of all materials are assumed independent of temperature. The whole body model is segmented into voxels with a resolution of 2×2×2 mm^3.

Gradient coils

Three sets of gradient coils, designed according to modern techniques (16,17) which allow obtaining complex shapes, are considered. The first one is a conventional system suitable for tubular MRI scanners; the magnitude of the gradient (G) and the diameter spherical volume (DSV) are 30 mT/m and 500 mm, respectively (Fig.2a). In the second set, designed to be used inside MRI-LINAC platforms (13), each axis is equipped with a couple of separated coils ("split coils"), so that a central gap is exploited during LINAC treatments. As shown in Figures 2b and 2c, besides the usual axial arrangement, this structure allows positioning the patient radially inside the gap (in this case the LINAC gun does not move, whereas the patient's body is rotated to reduce collateral effects of radiotherapy). The gradient coils are designed to produce a gradient G = 30 mT/m within a 300 mm DSV. Finally, a set of uniplanar coils, specifically used for scanning the spinal cord, is analyzed. These windings are designed to be positioned under the patient's back (Fig.2d) and they can produce a 50 mT/m gradient in a small region around the spine. The models of all sets of GC include the description of the x-, y- and z-coils, fed with impressed currents. A common switching sequence, with a main harmonic of 1 kHz, is assumed.

Numerical models

The electromagnetic-thermal field problem is decomposed into two successive solutions. The electromagnetic simulations are carried out through a non-commercial code, written in terms of electric vector potential and magnetic scalar potential (18-20) in the frequency domain. The equations are solved according to a hybrid Finite Element – Boundary Element Method (FEM-BEM) based on a combination of edge and nodal elements, where the known term is the magnetic field produced by the GC under unperturbed conditions (21), simulated via Biot-Savart relation. The code has been specifically conceived to optimize the computational burden, allowing the simulation of many cases in a relatively short time. Experimental and computational validation tests (22) were performed to check the electromagnetic code. In particular, calorimetric measurements applied (under adiabatic conditions) to a brass sample exposed to the 20 mT/m gradient field of the 3 T MRI scanner available at PTB, have proved the reliability of the software.

Preliminary analyses showed that the power deposition due to the electromagnetic field is almost completely confined inside the metallic implants (i.e. power deposition is negligible inside human tissues at the frequencies involved by GC. This means that the specific absorption rate (SAR), adopted by ICNIRP to assess the exposure above 100 kHz (23), results to be negligible in the current cases. Thus, the computational domain for the electromagnetic analysis is limited to the prostheses, which are not simulated as perfect conductors but with their finite electrical conductivity. During the simulations, a periodic sinusoidal driving current is used, so that the desired gradient magnitude is produced inside the DSV in correspondence of the peak of the sinusoid; then, the distribution of volume power density (P_{em}) due to Joule losses inside the implants is determined. For the sake of simplicity, all coils are energized simultaneously and in phase. Then, P_{em} is exploited as driving term for the thermal model described by the Pennes bioheat equation (24), which is applied to the human body (prostheses and tissues) to study the heat diffusion, accounting for the effect of blood perfusion. The thermal formulation, written in terms of temperature elevation and subject to Robin (convection) boundary conditions, is implemented into a non-commercial software based on FEM (13, 21). Throughout the computational scheme, P_{em} is kept constant and the distribution of temperature elevation at steady-state (Θ_{ss}), under thermal equilibrium, is computed. The reliability of the thermal code has been checked through comparisons with analogous results produced by the commercial software Semcad X (25), finding a satisfactory agreement (local discrepancies of a few percent, under the same P_{em} spatial distribution).

Scaling the results for sequences

The temperature elevation Θ_{ss} provided by the numerical model following the approach previously described (basic result) is an initial raw estimate of the temperature elevation that could occur during an MRI scan; but it is unscaled for sequence specifics. From one viewpoint, it is an underestimate, because the actual waveform of the GC signal is not sinusoidal (typically it is trapezoidal) and involves higher-order harmonics, whose contribution increases the temperature elevation. On the other hand, it is most likely a non-negligible overestimate, because it is obtained by considering a continuous exposure to the gradient switching field, without taking into account idle times and the limited duration of the exam. In order to produce a realistic prediction of the temperature elevation, the following procedure is applied to correct the aforementioned effects. First of all, the values of Θ_{ss}, computed here for specific values of G, can be adjusted to any other level by taking into account that Joule losses in the prostheses are proportional to G^2 and therefore, due to the linearity of the thermal problem with respect to P_{em}, Θ_{ss} scales as G^2 too. However, given the large number of sequences used in MRI scanners, it is not possible to explore all possible situations. Thus, for the sake of simplicity, the procedure is presented with reference to a generic switching sequence. The same scheme could be applied to any other pulse sequence used in practice.

The considered sequence is composed of a train of trapezoidal pulses, symmetric with respect to zero (so that positive and negative plateaus with magnitude G alternate continuously). The frequency of one complete trapezoidal wave (including a positive and a negative half-wave) is set to f = 1 kHz; this waveform is

repeated N times during an interval t_{on} and then the coils are switched-off for a time t_{off} (see Sup.Fig.S1). This sequence, whose total duration is $T = t_{on} + t_{off}$, is repeated periodically during the MRI scan. This means that intervals in which Joule losses are produced inside the prostheses alternate with intervals without heat source, according to a duty-cycle $D = t_{on}/T$. As will be shown in the next Section (see Fig.7b), at a small time-scale this process gives rise to a succession of heating/cooling thermal transients, which have been reproduced through a specific algorithm developed in Matlab (26) environment. Nevertheless, on a gross time-scale the temperature elevation follows approximately the typical asymptotic response of a 1st-order system stimulated by a step function:

$$\theta_D(t) = \Theta_\infty \left(1 - e^{-t/\tau}\right) \qquad [1]$$

where t is time and the asymptotic "final" temperature elevation results to be $\Theta_\infty \cong D \cdot \Theta_{ss}$. The parameter τ in Eq.1 is the time constant of the transient evolution. Its value varies from point to point in a complex system like the human model and therefore it is not possible to provide specific material-dependent τ values. However, simulations performed with the thermal transient solver of Semcad X (using Joule losses distributions computed by the FEM-BEM code) suggest setting it between 8 and 10 minutes for tissues surrounding the prostheses. It must be noted that the gradient switching takes place on a much shorter time scale; hence, the succession of the above-mentioned heating/cooling processes introduces just small oscillations around the "average" evolution of temperature elevation. Thus, the knowledge of the duty-cycle D and of the total duration of the MRI scan (to be substituted for t in Eq.1), provides the first refinement in the estimate of the actual temperature elevation. The second step of the refinement aims at including the effect of the true waveform, which implicates higher-order harmonics. For the trapezoidal waveform here considered, it is easy to prove that the Fourier expansion involves only odd harmonics in phase among each other, whose amplitudes (negative in case of 180° phase shifts) are given by:

$$G_n = \frac{2G}{(n\pi)^2 f} \frac{1}{t_{slope}} \sin\left[(2n\pi f) t_{slope}\right] \qquad [2]$$

where t_{slope} is the time required to switch from zero to the positive (or negative) plateau, and vice versa, whereas n is the order of the harmonic (n = 1, 3, 5, 7, …). This means that the actual amplitude of the first harmonic (the sinusoid with frequency of 1 kHz) is not simply G, but it must be computed according to Eq.2. Since, as already explained, the temperature elevation depends on G^2, it has to be scaled according to $(G_1/G)^2$ for the first harmonic. To account for other harmonics, the simulations must be repeated by feeding the GC with sinusoidal currents at the proper frequency (3 kHz, 5 kHz, 7 kHz,… in the present study), producing inside the DSV a gradient magnitude equal to G in correspondence of the current peak. These simulations, performed up to n = 7, have shown that the spatial distribution of the maxima of both P_{em} and temperature elevation remains almost unchanged for all the considered harmonics (compare for example Fig.3b with Sup.Fig.S2). Since the superposition principle applies to temperature elevation with respect to the power density of each single harmonic, the estimate can be further refined by adding the corresponding terms, each one scaled according to the ratio $(G_n/G)^2$ (which makes negative signs irrelevant):

$$\theta(t)=\theta_D(t)\left[\left(\frac{G_1}{G}\right)^2+k_3\left(\frac{G_3}{G}\right)^2+k_5\left(\frac{G_5}{G}\right)^2+k_7\left(\frac{G_7}{G}\right)^2\right]=\frac{\theta_D(t)}{G^2}\left(G_1^{\,2}+k_3G_3^{\,2}+k_5G_5^{\,2}+k_7G_7^{\,2}\right) \qquad [3]$$

In absence of skin effect, coefficients k_3, k_5, k_7 would be equal to 9, 25 and 49 (i.e. the square of the harmonic order), respectively. Indeed, the induced electric field would be simply proportional to frequency (27) while P_{em} is proportional to the square of such field. In reality, owing to the skin effect, their values result to be lower. For the cases under analysis, it has been verified empirically that they can be reasonably set to 6, 10 and 14, respectively. Note that this last refinement leads approximately to the same result as performing the simulations using, for each harmonic, a current amplitude equal to the actual one (given by the Fourier expansion of the true current waveform), adding all contributions to get the total P_{em}, and solving one single thermal problem with this latter "cumulative" power density as input.

RESULTS

The temperature rises are calculated firstly in a continuous exposure situation and later they will be scaled for realistic sequences. Figure 3 shows the results obtained for a unilateral CoCrMo implant exposed to the conventional GC set. The temperature elevations have been obtained by considering only the first harmonic (1 kHz), whose peak produces a gradient magnitude of 30 mT/m (i.e. the basic results). Fig.3a presents the maximum values of the raw temperature elevation computed at steady-state (Θ_{ss}) in the metal and in four biological materials (bone, fat, marrow red and muscle) that are close to the implant, and therefore result to be the hottest tissues. The axial position of the body is indicated by Δ. $\Delta = 0$ means that the top of the femur lies in correspondence of the GC center; a positive or negative value of Δ indicates that the body is shifted longitudinally in the direction of the head or of the feet, respectively. Fig.3b shows the spatial distribution of Θ_{ss} when $\Delta = -300$ mm (i.e. the worst case), in a generic coronal section of the body.

Analogous results are reported in Fig.4 for the bilateral implant, considering both the CoCrMo and Ti-6Al-4V alloys (Figs.4a and 4b, respectively). As can be seen, they are qualitatively similar, but the maxima Θ_{ss} for the unilateral implant are about 80 % of the ones computed for the bilateral CoCrMo implant. Fig.4c shows a map of Θ_{ss} for the CoCrMo alloy at $\Delta = -300$ mm (i.e. the worst case), in a generic coronal section, where the trace of the right implant appears to be hotter than the left one (the pelvis of the human model is slightly rotated). Since a similar behavior has been found in all the analyzed cases, only results obtained with the bilateral implant will be shown in the following.

The results obtained for the split coils are given in Fig.5, for both CoCrMo and Ti-6Al-4V alloys. The analysis is performed for three possible arrangements of the body: axial, radial with the back facing the floor (similar to the position shown in Fig.2b) and radial with one side facing the floor (see Fig.2c). Also in these cases Δ indicates a longitudinal shift with respect to the reference position (top of the femoral head in the center of the GC).

Finally, Fig.6 shows the results obtained with the body lying over the uniplanar coils, as sketched in Fig.2d, at two different distances from them (54 mm and 74 mm, measured from the back of the body to the bottom of the coil envelope). Both metallic alloys have been considered. A histogram comparing the maximum Θ_{ss}

found in biological tissues throughout Figs.3-6 is available online (Sup.Fig.S3). A picture (Sup.Fig.S4) indicating the position of the human body with respect to the isocentre for the worst cases is also available for conventional and split coils (for the uniplanar coils, the position of the isocentre can be directly deduced from Fig.2d).

As already explained, the results in terms of Θ_{ss} (which are consistent with the preliminary analyses presented by the authors in (11) and (13)) must be refined to find more realistic temperature elevation values. This can be done by defining the features of the switching sequence. To provide an example, a set of parameters similar to the one of a diffusion weighted single shot planar echo sequence is considered: N = 40, t_{on} = 40 ms, T = 200 ms, D = 0.2, t_{slope} = 125 μs (see Sup.Fig.S1). The example is developed for the exposure scenario reported in Fig.3 with $\Delta = -300$ mm, and specifically for the hottest point in a biological tissue (in muscle, where maximum Θ_{ss} is equal to 14.4 °C). For this point, the time evolution of the raw temperature elevation (computed through the thermal transient solver of Semcad X, using as input the spatial distribution of P_{em} determined through the FEM-BEM software), is given in Fig.7a. An approximation of such behavior, obtained through an analytic exponential function setting empirically the time constant to 540 s, is also shown in the same picture. This value has been used for τ within the Matlab code, to get the time evolution of the temperature elevation refined according to the duty-cycle (θ_D). It is shown in Fig.7b, together with a zoom, which puts in evidence the oscillation occurring at a small time scale due to the succession of on/off heating phases.

Then, the refinement requires the computation of the Fourier expansion of the true switching waveform. Given the nominal gradient magnitude G = 30 mT/m, according to relation [2] the amplitude of the first, third, fifth and seventh gradient harmonics are respectively G_1 = 34.4 mT/m, G_3 = 3.82 mT/m, G_5 = 1.38 mT/m, G_7 = 0.0702 mT/m. Finally, by exploiting the empirical relation [3] to rescale the curve of Fig.7b, and choosing a realistic scanning time of 30 minutes, the maximum temperature elevation for the considered case results to be $\theta(t = 1800\text{ s}) \cong 4$ °C.

DISCUSSION AND CONCLUSIONS

The results obtained for the unilateral implant are qualitatively similar to the ones of the bilateral implant, but smaller in magnitude (due to the features of the single prostheses and not to their number). Moreover, the histograms indicate that the Ti-6Al-4V alloy (having lower electric and thermal conductivities) produces results analogous to those obtained for the CoCrMo alloy, but these latter are generally about 1.5 - 2 times higher and therefore represent the worst case. Speaking about conventional GC, Θ_{ss} is relatively low for the reference position (with prostheses located within the central scanning volume), whereas it increases up to a maximum when the body is shifted thereabout to $\Delta = \pm 300$ mm. A further shift results in a decrease of temperature elevation (note that a position outside the range −600 mm to +300 mm would be meaningless for MRI purposes). As regards split coils, the results obtained with the axial arrangement are qualitatively similar to those found with conventional GC; the same occurs in the radial arrangement with one side facing the floor. On the contrary, if the back is facing the floor in radial arrangement, the worst case is found when

$\Delta = -150$ mm. During an MRI-LINAC treatment, with the body rotating around its own axis in radial position, an estimate of the raw temperature elevation could be obtained as an average of the values given in Fig.5c (or 5d) and Fig.5e (or 5f), considering a reasonable rotation period on the order of 1 minute (quite small with respect to the time constant τ). Among all the configurations with split coils, the traditional axial arrangement produces the highest temperature, but it is smaller than that obtained with conventional coils. Despite the high gradient magnitude, the uniplanar coils induce lower Θ_{ss}, because such a high gradient occurs in a quite small volume and does not involve the metallic implants.

In all cases, as suggested by Fig.3b, the heating process involves a limited region around the prostheses. Outside this volume, the temperature elevation is very small, indicating that practically, the thermal diffusion is mainly controlled by local blood perfusion.

The "rule of thumb" proposed to refine the estimate deserves the last comments. The approach is clearly approximated, because the actual time evolution is not a perfect exponential curve, making the identification of the time constant not so straightforward. Moreover, τ is a function of position, and this means that the maximum temperature elevation may occur at different points for different time values. However, due to the intrinsic uncertainty associated with this kind of estimate (coming from the large variability in the features of body size, tissue properties, prostheses, MRI scanners and switching sequences), it is not appropriate to try to present extremely specific results. Thus, the procedure presented here is relatively simple and general enough to provide a practical approach, which could be applied systematically to inform safety guidelines. In the example proposed above, the first unscaled estimate changes from 14.4 °C to 4 °C, taking into account realistic sequence parameters. This estimate would reduce to 3.64 °C if just the contribution of the first harmonic were included in relation [3] (it would be 2.77 °C after the first refinement due to the duty-cycle, having simulated the trapezoidal wave through a sinusoid with the same peak). Results such as these indicate a possible concern for safety and put in evidence that further experimental investigations are needed.

ACKNOWLEDGMENTS

This work received funding from the Italian MIUR project "Metrology for therapeutic and diagnostic techniques based on electromagnetic radiation and ultrasound waves" (2014-2016) and from the European Metrology Research Programme (EMRP)-HLT06 Joint Research Project (JRP) "Metrology for next-generation safety standards and equipment in MRI" (2012–2015). EMRP is jointly funded by the EMRP participating countries within EURAMET and the European Union. The authors acknowledge the contribution of A. Papadaki in providing voxel data of hip prostheses

REFERENCES

1. Organisation for Economic Co-operation and Development (OECD). Health at a glance 2013: OECD Indicators. Paris: OECD Publishing). http://dx.doi.org/10.1787/health_glance-2013-en. Published November 21, 2013. Accessed October 24, 2014.

2. Hargreaves BA, Worters PW, Butts Pauly K, Pauly JM, Koch KM, Gold GE. Metal-induced artifacts in MRI. A.J.R. 2011;390:547–555.
3. Liu F, Xia L, Crozier S. Influence of magnetically-induced E-fields on cardiac electric activity during MRI: A modeling study. Magn. Reson. Med. 2003;50:1180–1188.
4. Feldman R, Odegaard J, Handler WB, Blaine AC. Simulation of head-gradient-coil induced electric fields in a human model. Magn. Reson. Med. 2012;68:1973–1982.
5. Schaefers G, Kugel H. A basic investigation of heating effects on total hip prostheses in combination with a simulated skin contact of the inner thighs during magnetic resonance imaging (MRI) with an 1.5 Tesla MR system. In Proceedings of the ISMRM Workshop on MRI Safety: Update, Practical Information and Future Implications, McClean, Virginia, USA, 2005.
6. Stenschke J, Li D, Thomann M, Schaefers G, Zylka W. A numerical investigation of RF heating effect on implants during MRI compared to experimental measurements. Adv. Med. Eng. 2007;114:53–58.
7. Mohsin SA, Sheikh NM, Abbas W. MRI induced heating of artificial bone implants. J. Electromagnet. Wave. 2009;23:799–808.
8. Powell J, Papadaki A, Hand J, Hart A, McRobbie D. Numerical simulation of SAR induced around Co-Cr-Mo hip prostheses in situ exposed to RF fields associated with 1.5 and 3 T MRI body coils. Magn. Reson. Med. 2012;68:960–968.
9. Abbasi M, Schaefers G, Sánchez JD, Erni D. Worst-case analysis of RF-induced heating during MRI scanning in a generic multicomponent orthopedic medical implant applying the design of experiment method (DOE). In Proceedings of the Joint Annual Meeting ISMRM-ESMRMB, Milan, Italy, 2014. p.4866.
10. Graf H, Steidle G, Schick F. Heating of metallic implants and instruments induced by gradient switching in a 1.5 T whole body unit. J. Magn. Reson. 2007;26:1328–1333.
11. Sanchez Lopez H, Zilberti L, Bottauscio O, Hand J, Papadaki A, Tang F, Chiampi M, Crozier S. Heating of bilateral hip prosthesis in a human body model induced by a multi-axis gradient coil set. In Proceedings of the Joint Annual Meeting ISMRM-ESMRMB, Milan, Italy, 2014. p.4878.
12. Raaymakers BW, Lagendijk JJW, Overweg J, et al. Integrating a 1.5 T MRI scanner with a 6 MV accelerator: proof of concept. Phys. Med. Biol. 2009;54:N229–N237.
13. Zilberti L, Bottauscio O, Chiampi M, Hand J, Sanchez Lopez H, Crozier S. Collateral thermal effect of MRI-LINAC gradient coils on metallic hip prostheses. IEEE T. Magn. 2014;50:5101704.
14. Christ A, Kainz W, Hahn EG, et al. The Virtual Family-development of surface-based anatomical models of two adults and two children for dosimetric simulations. Phys. Med. Biol. 2010;55:N23–N38.
15. P. Hasgall et al., IT'IS Database for thermal and electromagnetic parameters of biological tissues. http://www.itis.ethz.ch/database. Version 2.4, July 2013. Accessed October 24, 2014.
16. Sanchez Lopez H, Poole MS, Crozier S. An improved equivalent magnetization current method applied to the design of local breast gradient coils. J. Magn. Reson. 2009;199:48–55.

17. Poole MS, While PT, Sanchez Lopez H, Crozier S. Minimax current density gradient coils: Analysis of coil performance and heating. Magn. Reson. Med. 2012;68:639–648.
18. Bouillault F, Ren Z, Razek A. Calculation of 3D eddy current problems by an hybrid T-Ω method. IEEE T. Magn. 1990;26:478–481.
19. Krakowski MR. Some theorems of the eddy-current theory. Archiv für Elektrotechnik. 1991;74:329–334.
20. Biro O, Preis K, Renhart W, Vrisk G, Richter KR. Computation of 3-D current driven skin effect problems using a current vector potential. IEEE T. Magn. 1993;29:1325–1328.
21. Bottauscio O, Chiampi M, Hand J, Zilberti L. A GPU Computational Code for Eddy-Current Problems in Voxel-Based Anatomy. To appear on IEEE T. Magn. DOI: 10.1109/TMAG.2014.2363140.
22. Giordano D, Zilberti L, Borsero M, Chiampi M, Bottauscio O. Experimental Validation of MRI Dosimetric Simulations in Phantoms Including Metallic Objects. IEEE T. Magn. 2014;50:5101504.
23. International Commission on Non-Ionizing Radiation Protection. Guidelines for limiting exposure to time-varying electric, magnetic, and electromagnetic fields (up to 300 GHz). Health Phys. 1998;74:494–522.
24. Pennes HH. Analysis of tissue and arterial blood temperatures in the resting human forearm. J Appl. Physiol. 1948;1:93–122.
25. SPEAG. http://www.speag.com/products/semcad/solutions/med. Accessed October 24, 2014.
26. MathWorks. http://www.mathworks.com. Accessed October 24, 2014.
27. International Electrotechnical Commission. Technical Standard IEC 62226-2-1: Exposure to electric or magnetic fields in the low and intermediate frequency range - Methods for calculating the current density and internal electric field induced in the human body - Part 2-1: Exposure to magnetic fields. http://webstore.iec.ch/. Published November 23, 2004. Accessed January 21, 2015.

LIST OF FIGURE CAPTIONS

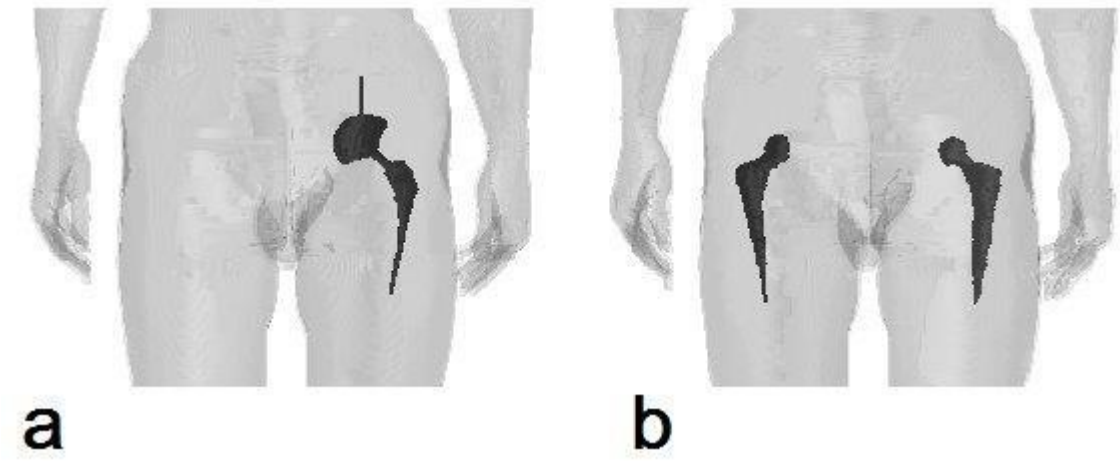

FIG.1. Pelvis of the human model with unilateral (a) and bilateral (b) hip implants. Both pictures are taken at the back of the model.

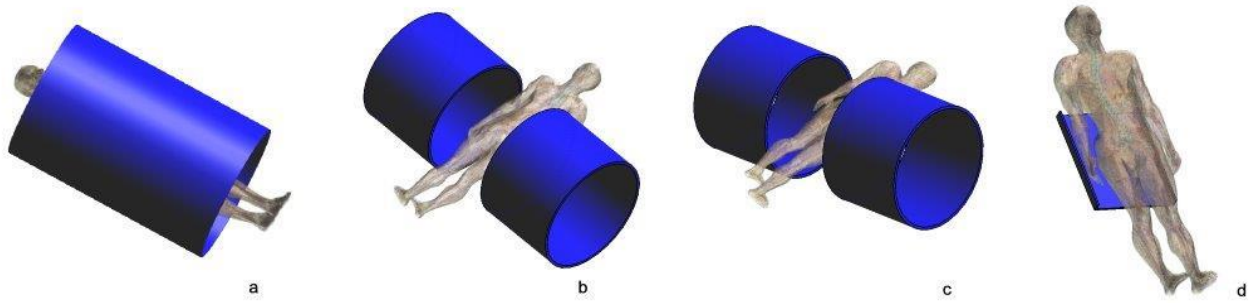

FIG.2. Human model disposed (a) longitudinally inside conventional gradient coils or radially between split coils for MRI-LINAC treatment, with (b) the back facing the floor or (c) one side facing the floor; (d) human model lying over uniplanar coils.

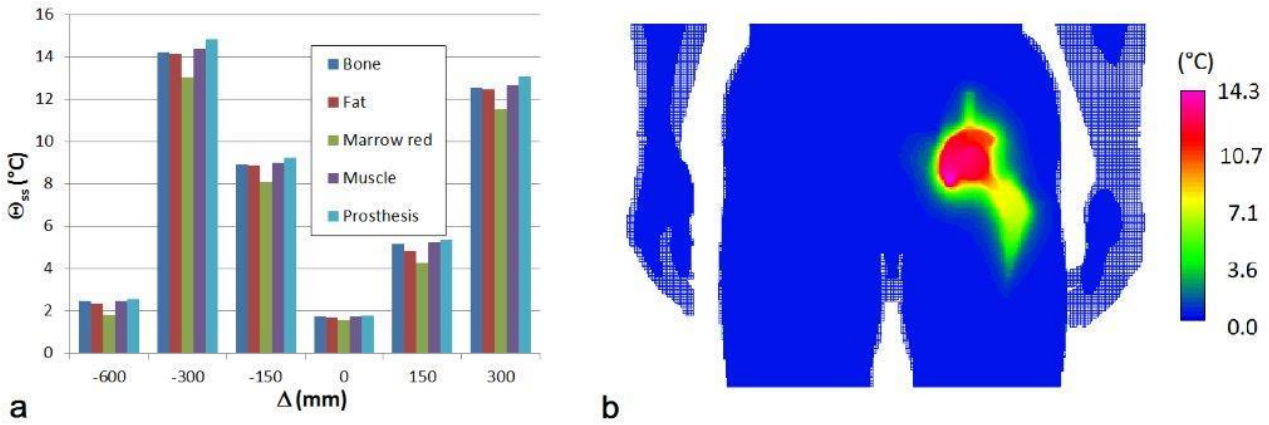

FIG.3. Raw steady-state temperature elevation for a CoCrMo unilateral implant in conventional GC: (a) maximum values as a function of body position; (b) color map in a generic coronal section for $\Delta = -300$ mm.

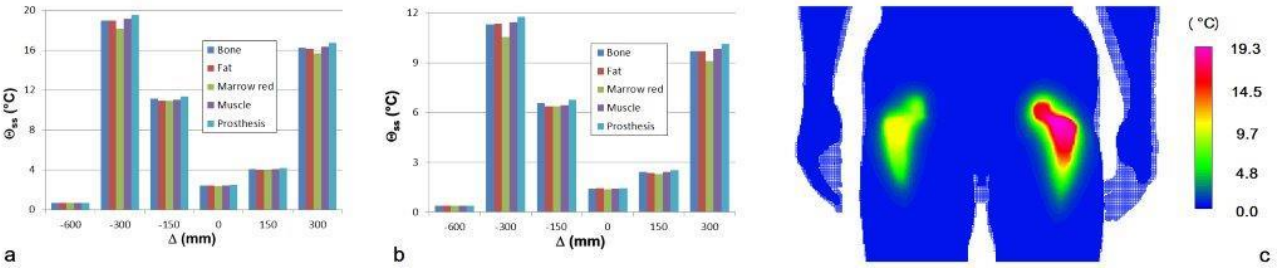

FIG.4. Raw steady-state temperature elevation for a bilateral implant in conventional GC: (a) maximum values as a function of body position for the CoCrMo alloy; (b) maximum values as a function of body position for the Ti-6Al-4V alloy; (c) color map in a generic coronal section for the CoCrMo alloy and $\Delta = -300$ mm.

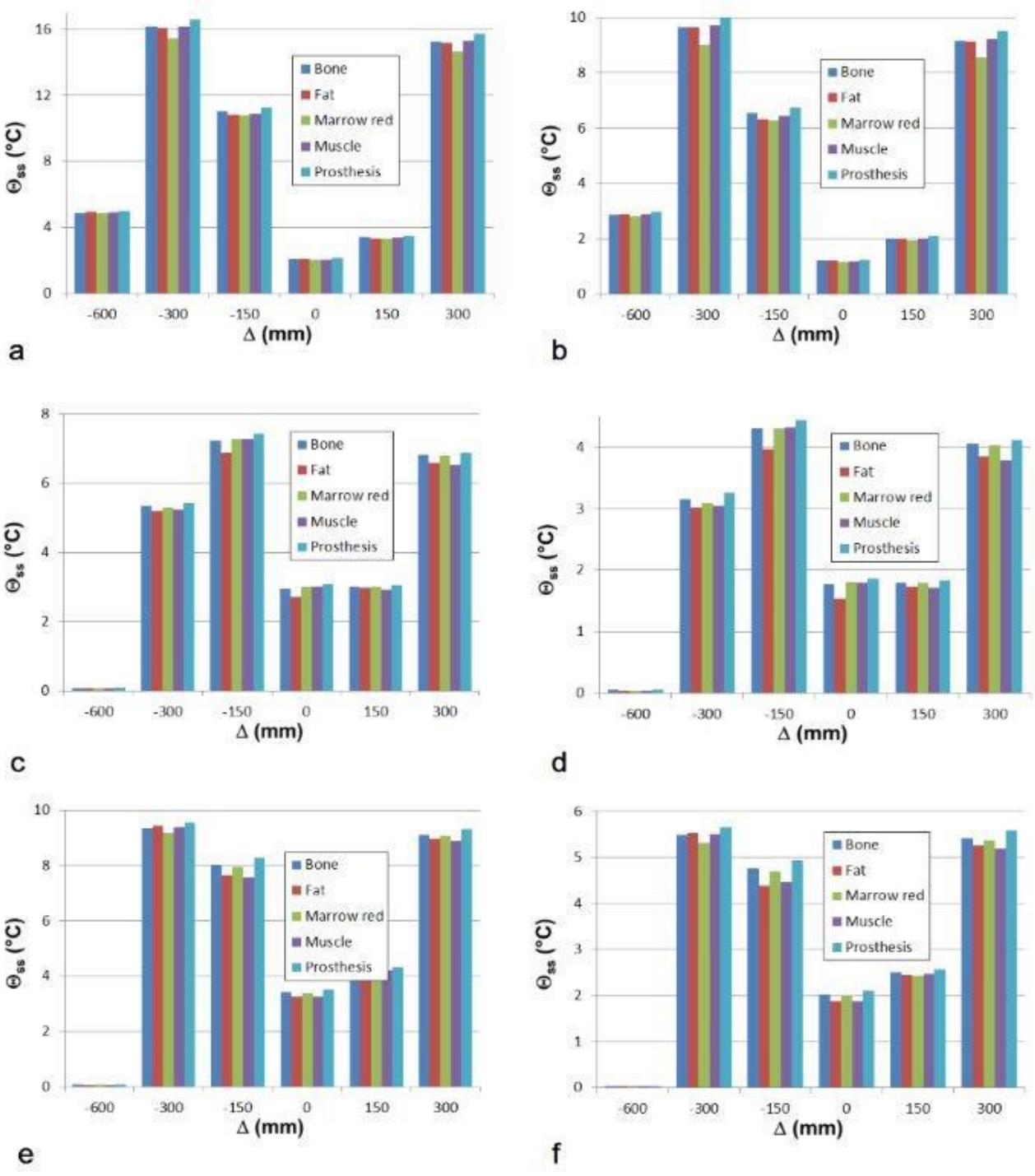

FIG.5. Raw temperature elevation computed at steady-state for a bilateral implant in split coils used for MRI-guided LINAC treatments: (a) CoCrMo alloy, axial position; (b) Ti-6Al-4V alloy, axial position; (c) CoCrMo alloy, radial position with the back facing the floor; (d) Ti-6Al-4V alloy, radial position with the back facing the floor; (e) CoCrMo alloy, radial position with one side facing the floor; (f) Ti-6Al-4V alloy, radial position with one side facing the floor.

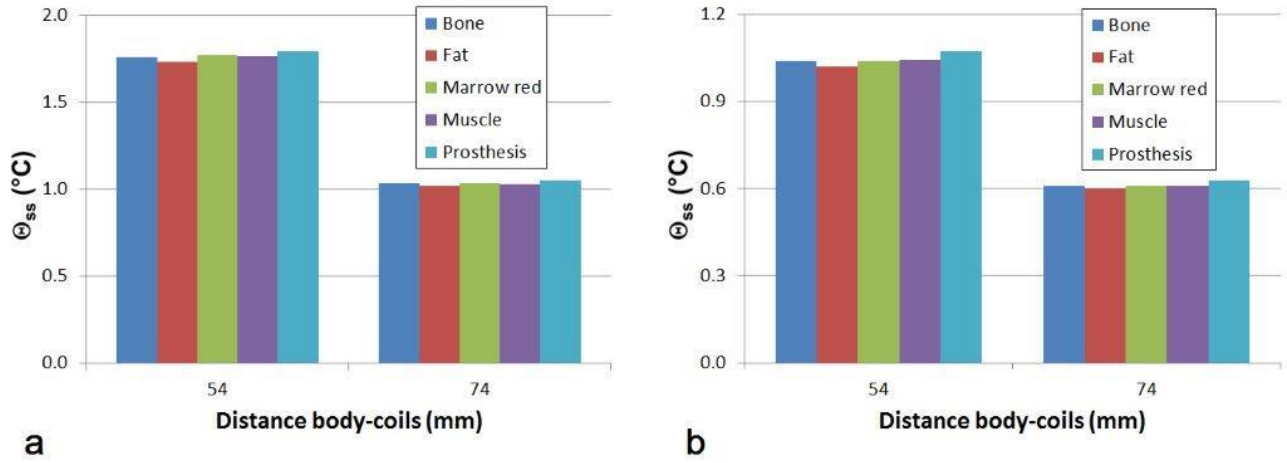

FIG.6. Raw temperature elevation computed at steady-state for a bilateral implant and uniplanar spinal coils: (a) CoCrMo alloy; (b) Ti-6Al-4V alloy.

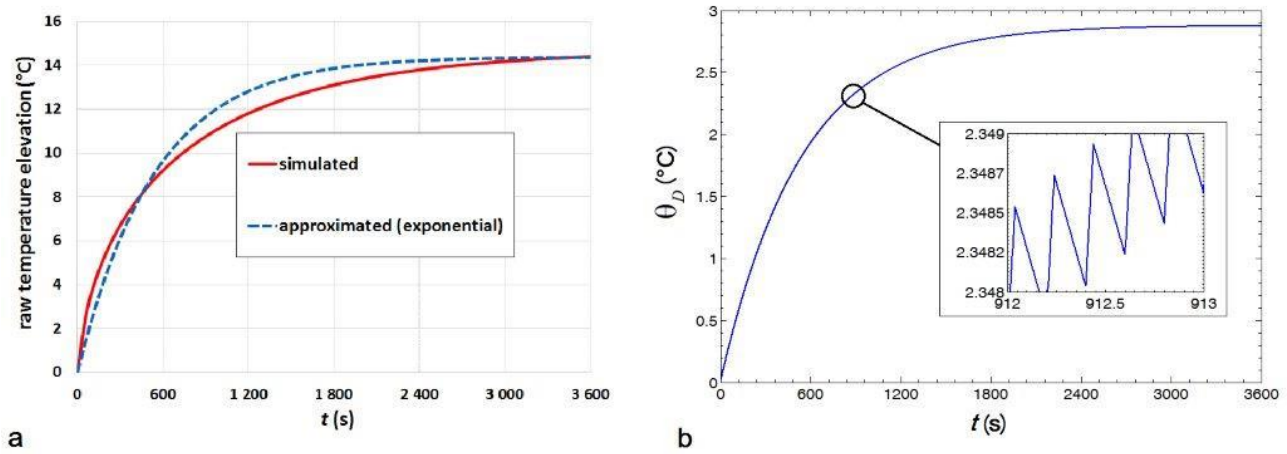

FIG.7. Time behavior of the temperature elevation investigated in Fig.3, with $\Delta = -300$ mm, for the point where the maximum heating takes place: (a) approximation of the simulated evolution through an exponential curve with $\tau = 540$ s; (b) temperature elevation after the refinement due to the duty-cycle (the inset puts in evidence the oscillating behavior at a small time scale).

LIST OF SUPPLEMENTARY MATERIALS

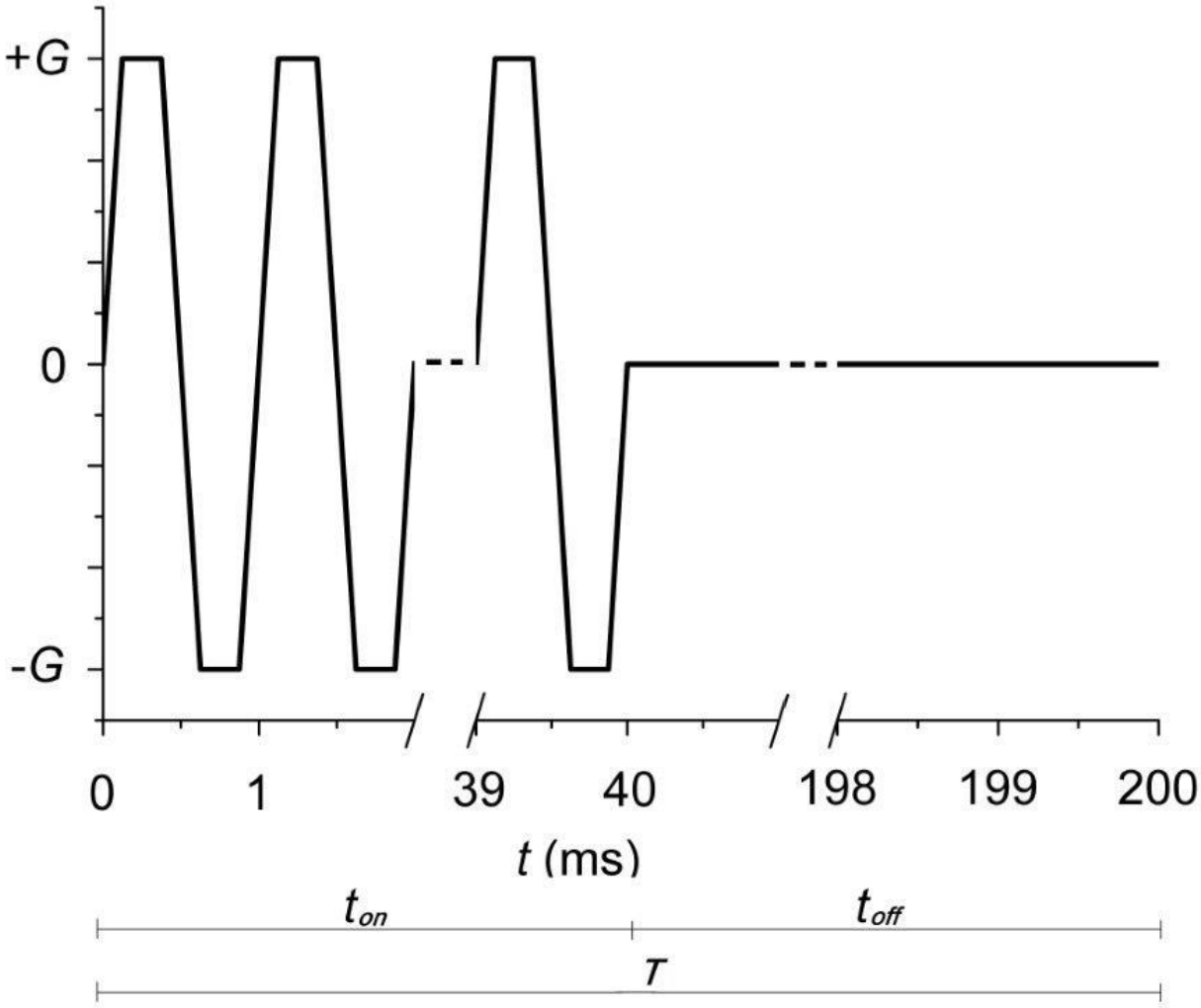

SUP.FIG.S1. Generic switching sequence adopted in the analysis, with indication of quantities t_{on}, t_{off} and T. Note that the axis of time has been broken at two points to fit the scale.

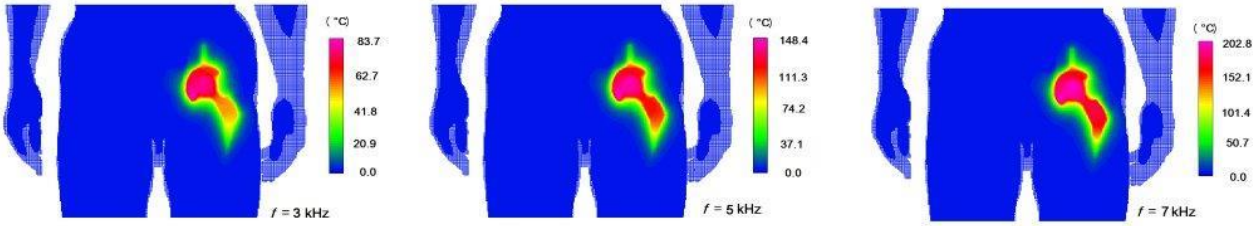

SUP.FIG.S2. Color maps (over a generic coronal section) of the raw steady-state temperature elevation for a CoCrMo unilateral implant in conventional GC at $\Delta = -300$ mm, obtained by simulating the exposure to the harmonics at 3 kHz, 5 kHz and 7 kHz. Please, pay attention because these values of temperature increase would be obtained if the peaks of the harmonics were equal to G (actually they must be rescaled according to equation [3]).

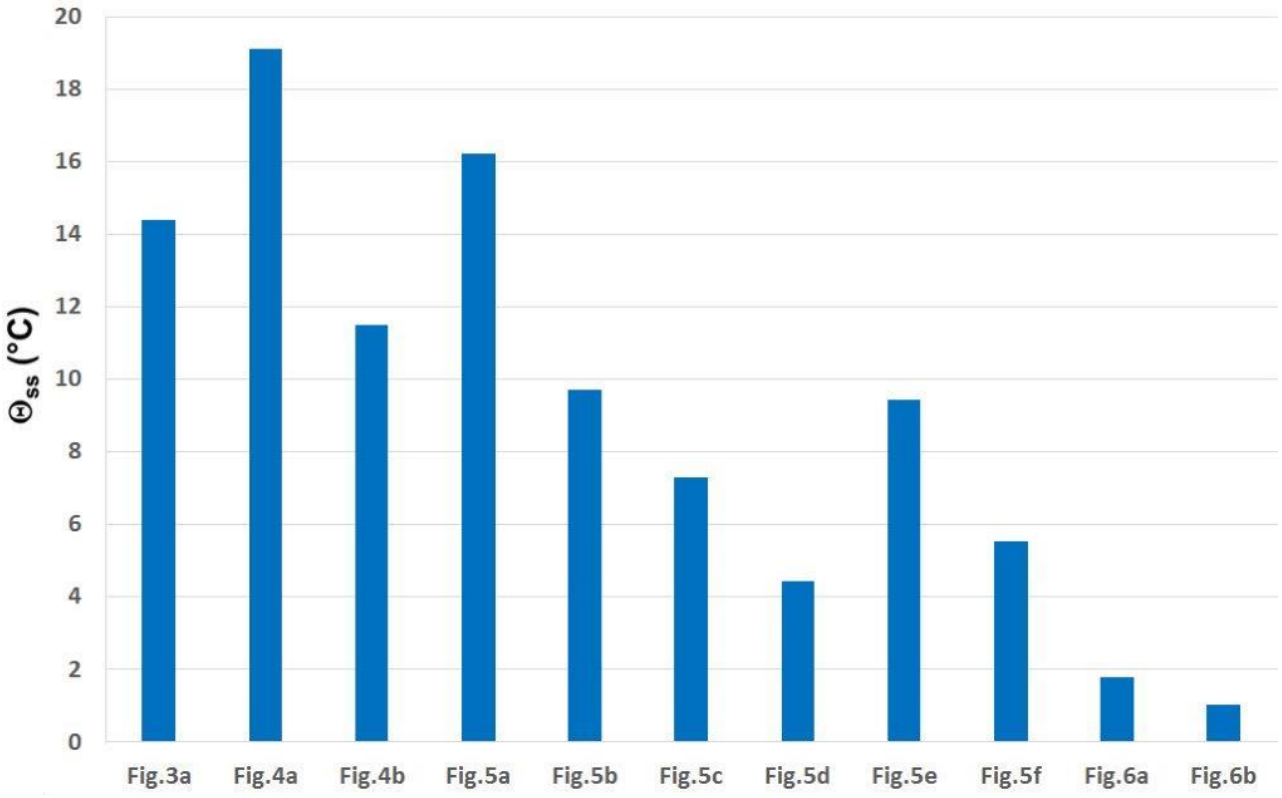

SUP.FIG.S3. Maximum values of the steady-state temperature elevation found throughout Figs. 3-6.

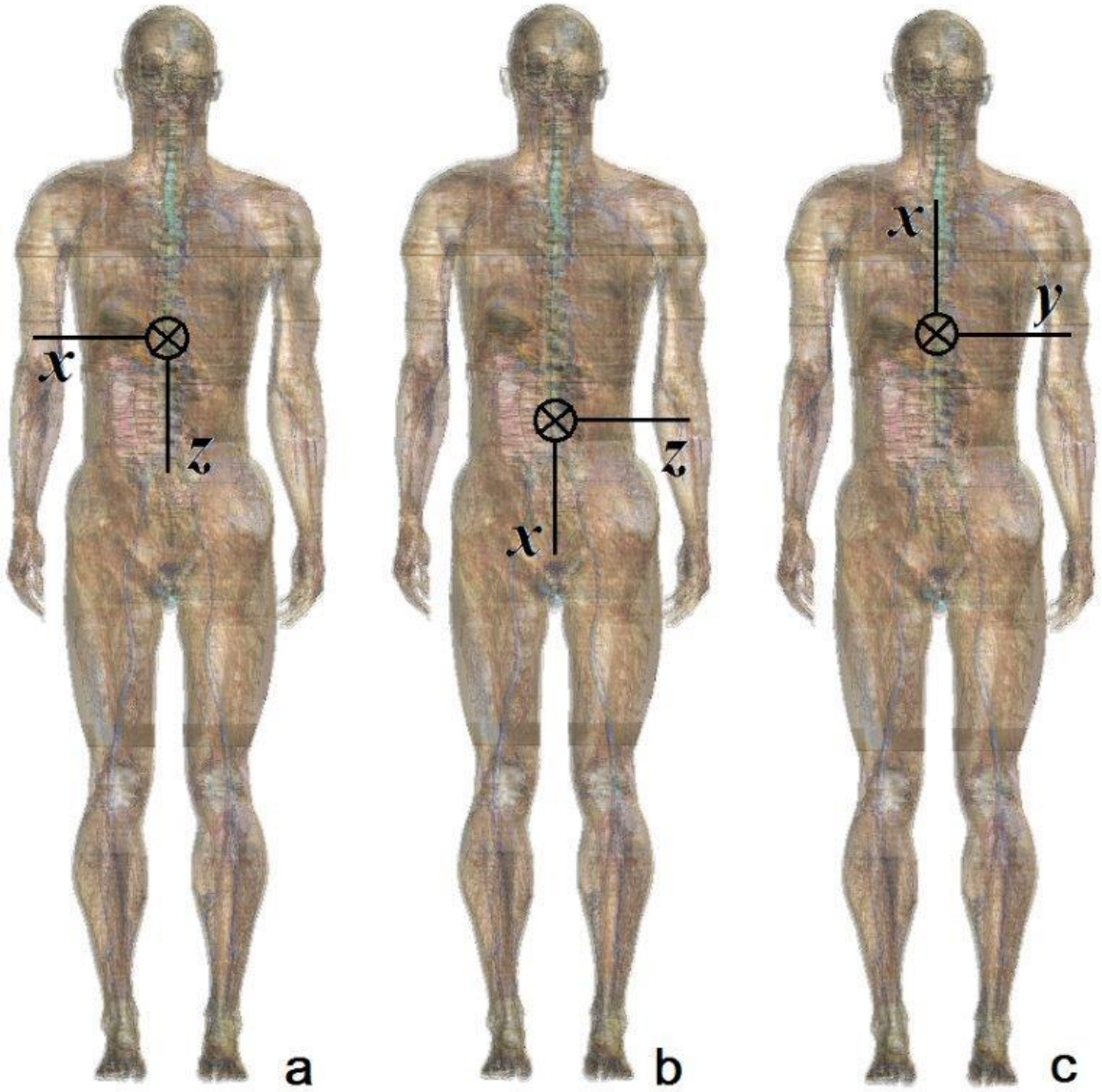

SUP.FIG.S4. Relative position of the human body with respect to the isocentre for the worst cases found throughout Figs. 3-5: (a) indication valid for conventional coils or split coils and axial arrangement; (b) indication valid for split coils and radial arrangement, when the back is facing the floor; (c) indication valid for split coils and radial arrangement, when one side is facing the floor. The position of the isocentre for the exposure cases involving the uniplanar coils can be directly deduced from Fig.2d.